Operando Spectroscopic Analysis of CoP Films Electrocatalyzing the Hydrogen-Evolution Reaction

Fadl H. Saadi[†,‡,✰], Azhar I. Carim[§,✰], Walter Drisdell[‡,#], Sheraz Gul[#], Jack H. Baricuatro[‡], Junko Yano[‡,#,*], Manuel P. Soriaga[‡,*], and Nathan S. Lewis[‡,§,ǁ,⊥,*]

[†]Division of Engineering and Applied Sciences, [‡]The Joint Center for Artificial Photosynthesis, [§]Division of Chemistry and Chemical Engineering, [ǁ]Kavli Nanoscience Institute, [⊥]Beckman Institute, California Institute of Technology, Pasadena, California 91125, United States.

[#]Molecular Biophysics and Integrated Bioimaging Division, Lawrence Berkeley National Laboratory, Berkeley, CA 94720, United States.

Supporting Information Placeholder

ABSTRACT: Transition metal phosphides exhibit high catalytic activity towards the electrochemical hydrogen-evolution reaction (HER) and resist chemical corrosion in acidic solutions. For example, an electrodeposited CoP catalyst exhibited an overpotential, η, of $-\eta < 100$ mV at a current density of -10 mA cm^{-2} in 0.500 M H$_2$SO$_4$(aq). To obtain a chemical description of the material as-prepared and also while effecting the HER in acidic media, such electrocatalyst films were investigated using Raman spectroscopy and X-ray absorption spectroscopy both *ex-situ* as well as under *in-situ* and *operando* conditions in 0.500 M H$_2$SO$_4$(aq). *Ex-situ* analysis using the tandem spectroscopies indicated the presence of multiple ordered and disordered phases that contained both near-zero valent and oxidized Co species, in addition to reduced and oxygenated P species. *Operando* analysis indicated that the active electrocatalyst was primarily amorphous and predominantly consisted of near-zero-valent Co as well as reduced P.

The electrolytic decomposition of water to produce H$_2$ can provide a sustainable, carbon-neutral source of chemical fuel, provided that the input energy is obtained from a renewable source.[1,2] Electrolytic H$_2$ production can compensate for the intermittency of solar and wind resources by storing energy in hydrogen molecules, which could be used upon demand.[3]

At many non-noble-metal cathode surfaces, the electrochemical half-reaction for the electrolytic production of H$_2$ from water, the hydrogen-evolution reaction (HER), does not proceed effectively in acidic media. Hence energy inputs that substantially exceed the thermodynamic value (overpotentials, η) must typically be utilized to generate H$_2$ at rapid rates (i.e. current densities).[4-6] The discovery of active HER electrocatalysts comprised of inexpensive and earth-abundant materials is thus being vigorously pursued.[7-9] Ni metal and Ni alloys are effective HER catalysts in alkaline media, but are susceptible to chemical corrosion in acidic electrolytes.[10-12] Electrocatalysts that are stable under operation in acidic media could be integrated into devices that utilize proton-exchange membrane (PEM) technologies, which have advantages relative to device designs that operate in alkaline media, including lower ohmic loss, lower gas crossover, and production of H$_2$(g) under high pressure.[13]

Nanoparticulate Ni$_2$P is an effective, acid-stable HER catalyst.[14] This observation has prompted substantial, sustained efforts to synthesize and develop other transition metal phosphide materials and to engineer such materials for maximum catalytic HER activity.[15-19] Electrodeposited CoP films effect the HER at a current density of -10 mA cm^{-2} with $-\eta < 100$ mV in acidic solution (pH < 1).[20] Characterization of this material, as well as related metal phosphides, has relied principally upon *ex-situ* techniques that typically involve analysis in vacuum or laboratory ambients. Herein, electrodeposited CoP films have been investigated under *in-situ* and *operando* conditions using Raman spectroscopy and Co and P K-edge X-ray absorption spectroscopy (XAS), including analysis of the resulting X-ray absorption near-edge structure (XANES) and extended X-ray absorption fine structure (EXAFS) data.
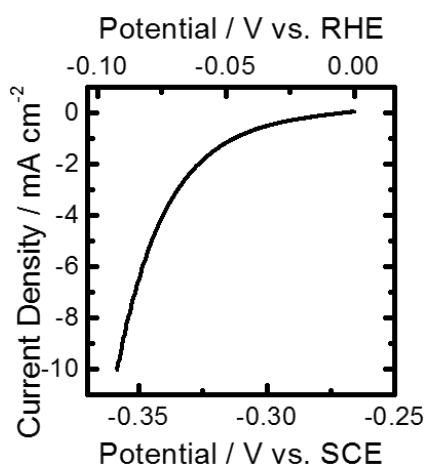
Figure 1. Cathodic polarization behavior of a CoP film in 0.500 M H_2SO_4(aq).

Electrocatalyst films were deposited potentiostatically onto planar Cu substrates, using an aqueous solution that contained $CoCl_2$ and $NaPO_2H_2$. Voltammetric, *in-situ,* and *operando* spectroscopic analyses were then performed in 0.500 M H_2SO_4(aq) (experimental methods are described in detail in the online Supporting Information). The steady-state voltammetric response (Figure 1) indicated that production of cathodic current densities of 0.5 and 10 mA cm^{-2} required overpotentials of -34 and -92 mV (applied biases of -0.300 V and -0.358 V vs. a saturated calomel electrode [SCE]), respectively (Figure 1). Figure 2a presents an *ex-situ* Raman spectrum of an as-deposited electrocatalyst film. The broad band centered at 595 cm^{-1} is indicative of amorphous cobalt oxide.[21] This band also exhibited shoulders at 477, 521, and 677 cm^{-1}, which correspond to Co_3O_4 phonon modes.[22] The Raman modes observed in the 970-1200 cm^{-1} spectral region are consistent with P-O stretching vibrations in a disordered system.[23,24] Prior X-ray photoelectron spectroscopic (XPS) analysis indicated the presence of Co metal, Co_3O_4, $Co_3(PO_4)_2$, as well as CoP in the as-deposited electrocatalyst film.[20] Moreover, the XPS analysis as well as prior energy-dispersive X-ray spectroscopic (EDS) analysis, indicated a Co:P elemental ratio in large excess of the 1:1 ratio expected for stoichiometric CoP, in accord with expectations that a substantial amount of Co species is not in the reduced phosphide state.[20] The Raman data presented herein are thus consistent with the prior XPS and EDS analyses.
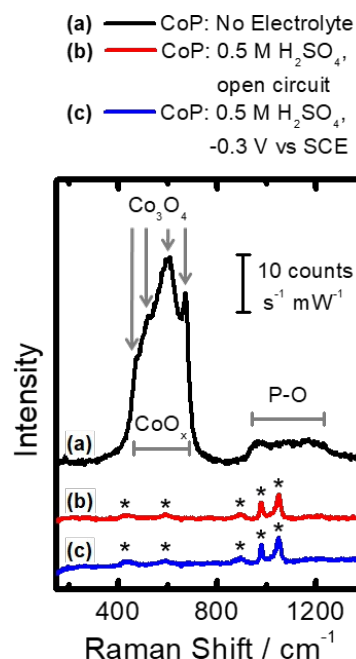
Figure 2. Raman spectra of CoP films. (a) Spectrum of a CoP film prior to contact with H_2SO_4(aq) (air ambient, *ex-situ*). (b) CoP film in 0.500 M H_2SO_4(aq) at open circuit (*in-situ*). (c) Same as (b) but at an applied potential of -0.300 V vs. SCE (*operando*). Spectral features consistent with amorphous CoO_x and crystalline Co_3O_4 phonon scattering and P-O stretching vibrations are labeled as such. * indicates spectral features consistent with scattering from the H_2SO_4(aq) electrolyte.

The same as-deposited electrocatalyst film was then immersed in 0.500 M H_2SO_4(aq) and an *in-situ* Raman spectrum was collected without an applied bias (open-circuit conditions; Figure 2b). The observed Raman modes centered at 429, 587, 896, 980, 1054 cm^{-1} are consistent with scattering from the aqueous H_2SO_4 electrolyte.[25,26] No other signals were observed, including those that correlated with oxidized Co and P species in the *ex-situ* Raman spectrum. After collection of the *in-situ* spectrum, a potential of -0.300 V vs. SCE was applied to the film such that the HER was being actively catalyzed, and an *operando* Raman spectrum was acquired (Figure 2c). The *operando* spectrum was nearly identical to the *in-situ* spectrum. Before and after collection of both the *in-situ* and *operando* spectra, substantial reflected excitation intensity was observed in a well-defined spot that was < 10 μm in diameter, consistent with the high numerical aperture of the objective in the Raman microprobe, indicating that the electrode interface was being interrogated throughout these analyses. Figure S1 presents an *ex-situ* Raman spectrum of crystalline CoP reference material, which exhibited several detectable signals at small Raman shifts consistent with phonon scattering in a crystalline material. The lack of observed phonon scattering in the *in-situ* and *operando* spectra is thus consistent with the amorphous nature of electrodeposited CoP as well as with the Pourbaix instability of oxidized cobalt species in strongly

acidic media.[20,27] Additionally, prior *ex-situ* XPS analysis of catalyst films after cathodic polarization in the HER regime in 0.500 M H_2SO_4(aq) displayed strong signals attributable to CoP while signals corresponding to both metallic and oxidized Co were not observed.[20] These XPS data, as well as analogous prior EDS data, also indicated a Co:P elemental ratio of 1:1, suggesting the removal of the elemental excess of Co observed using these techniques in the as-prepared film.[20] The film composition was thus consistent with the removal of the Pourbaix unstable metallic and oxidized Co species in 0.500 M H_2SO_4(aq). Hence, the results of the *in-situ* and *operando* Raman analysis are supported by the prior *ex-situ* XPS and EDS analyses after electrocatalytic operation.

To further elucidate the elemental oxidation states in the active electrocatalyst, Co K-edge and P K-edge XAS data were obtained in a manner analogous to the Raman investigation. The X-rays entered the electrochemical cell through the back of the catalyst film and thus provided a bulk probe of the entire film thickness. The acquired spectra thus represent the sum of signals originating from the material at the solution interface as well as all the material extending to the Cu substrate. This is similar to the Raman experiment where although the optical excitation was incident from the front towards the electrocatalyst-solution interface, the acquired spectra were derived from scatter generated both at and below the interface. Figure 3a-c presents representative *ex-situ*, *in-situ*, and *operando* Co K-edge X-ray absorption near-edge structure (XANES) spectra for the electrocatalyst films, with the data collected in a manner similar to the Raman spectra in Figure 2a-c. Figure 3d-e presents Co K-edge XANES spectra for Co metal and CoO standard materials. The *ex-situ*, *in-situ*, and *operando* spectra of the film all exhibited a pre-edge feature near 7711 eV that was similar to, but less intense than, that of the Co metal standard. This feature can be attributed to metal-to-ligand charge transfer, and resembles the pre-edge feature observed for Ni K-edge XANES spectra of Ni_2P.[28,29] The *ex-situ* spectrum also exhibited a white line feature at 7727 eV similar to that observed for the CoO standard material, indicating the presence of oxidized Co in the as-prepared material that was not detectable by XANES in the active electrocatalyst.

Figure 3f-j presents Fourier-transformed Co K-edge extended X-ray absorption fine structure (EXAFS) data analogous to the XANES data presented in Figure 3a-e. Due to the phase shift, the apparent distance in the Fourier-transformed data is ~0.5 Å shorter than the real distance.[30] A first-shell distance of ~2.30 Å (apparent distance ~1.8 Å) was observed for the catalyst was observed during *in-situ* (Figure 3g) and *operando* (Figure 3h) analysis, consistent with reported Co-P distances for amorphous Co-P alloys and crystalline Co_2P.[31-33] These distances are longer than the typical Co-O distance of ~2.12 Å (as shown in the CoO standard, apparent distance ~1.62 Å), implying direct Co-P interactions in the first shell.[34] The *in-situ* and *operando* EXAFS

provided no indication of long-range order (i.e. no peaks at distances >3 Å), suggesting that the catalyst is amorphous under these conditions. The lack of signals indicative of crystallinity is consistent with the Raman spectra. The *ex-situ* catalyst displayed a slightly different EXAFS pattern (Figure 3f), consistent with a CoP structure mixed with some metallic and oxidized Co as seen by comparison to Co foil and Co oxide standards. The evidence for oxidized Co species in the *ex-situ* data is also in accord with the Raman analysis.
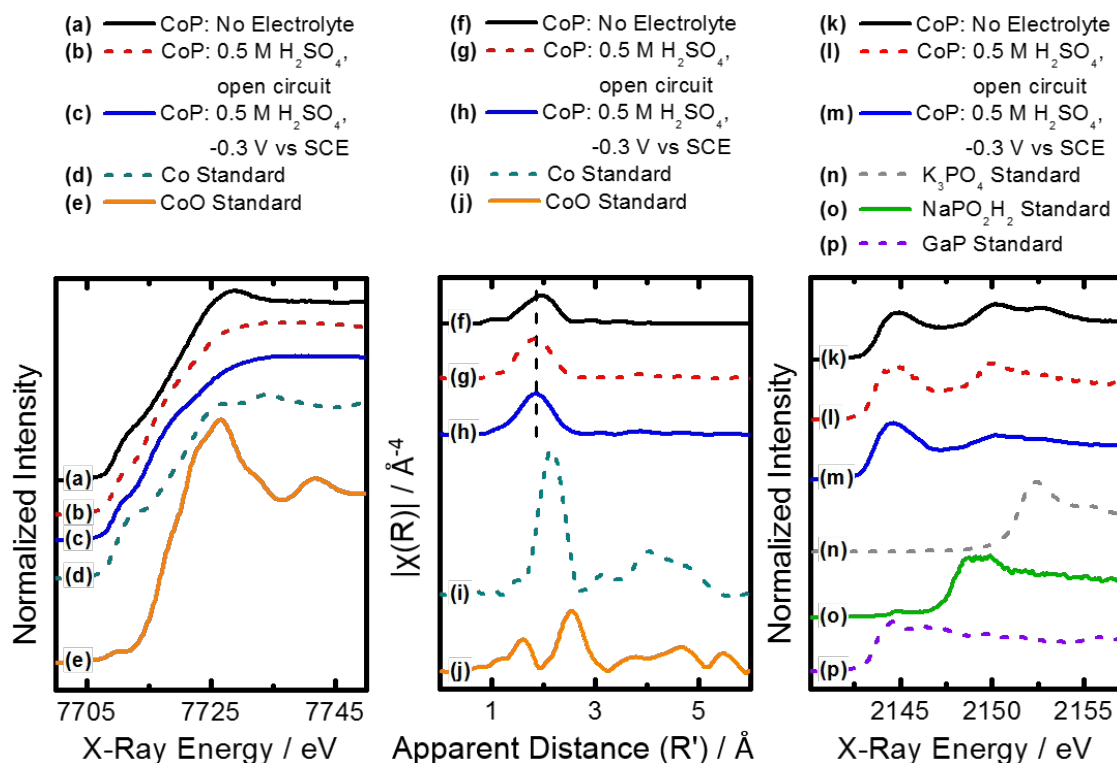
Figure 3. Co K-edge X-ray absorbance nea-edge spectra (XANES) of both CoP films under the indicated conditions and related spectral standards. (a) Spectrum of a CoP film prior to contact with H_2SO_4(aq) (air ambient, *ex-situ*). (b) CoP film in 0.500 M H_2SO_4(aq) at open circuit (*in-situ*) (dashed line centered at local spectral maximum). (c) Same as (b) but at an applied potential of -0.300 V vs. SCE (*operando*). (d) Co and (e) CoO standards. Fourier-transformed Co K-edge extended X-ray absorbance fine structure (EXAFS) data (f)-(j) analogous to the XANES data presented in (a)-(e). P K-edge XANES spectra (k)-(m) analogous to the XANES spectra presented in (a)-(c), and of (n) K_3PO_4, (o) $NaPO_2H_2$, and (p) GaP standards.

(a) *Ex-situ*

(b) *Operando*
0.5 M H_2SO_4, -0.3 V vs. SCE
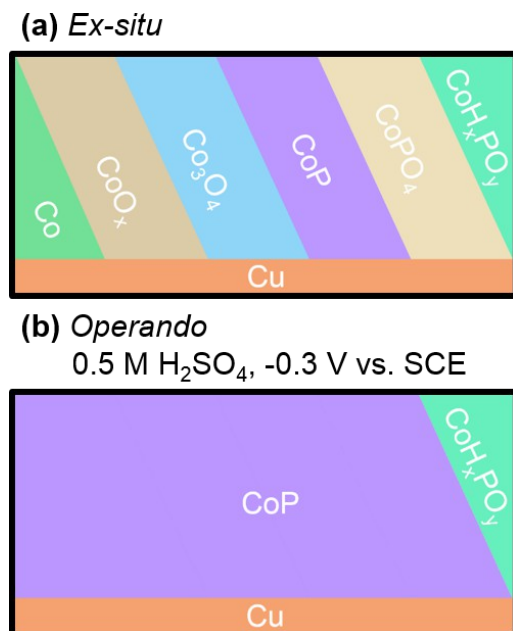
Figure 4. Graphical depictions of the composition of the electrodeposited catalyst film as derived from the cumulative (a) *ex-situ* analysis as well as from (b) *operando* analysis in 0.500 M H_2SO_4(aq) at an applied potential of -0.300 V vs. SCE.

Figure 3k-m presents P K-edge XANES spectra that are directly analogous to the Co K-edge XANES spectra presented in Figure 3a-c.

Additionally, Figure 5d-f displays the P K-edge XANES spectra for K_3PO_4, $NaPO_2H_2$ and GaP standard materials. The *ex-situ* electrocatalyst spectrum exhibited three major features which were centered at 2144.9, 2150.2 and 2152.6 eV, respectively. The feature at 2144.9 eV is a close match to that of the GaP standard, and is consistent with the presence of CoP. The feature at 2152.6 eV is a close match to the K_3PO_4 standard, and is consistent with the presence of a phosphate species in the as-deposited material. The feature at 2150.2 eV is consistent with a phosphorous species having an oxidation state intermediate between phosphide and phosphate. This feature is close to, but not an exact match with, the $NaPO_2H_2$ standard. This standard was unstable under the X-ray excitation, decomposing into a phosphate species that exhibited a characteristic spectral feature near 2152.2 eV as well as a phosphide with a characteristic spectral feature near 2144.9 eV (see Supporting Information for details). This instability precluded definitive determination of the precise energy of the $NaPO_2H_2$ spectral feature, but suggests a value of ~2149.4 eV. The as-prepared film may contain P in an oxidation state intermediate between that of it in $NaPO_2H_2$ and in K_3PO_4. Hence, the P K-edge XANES spectra indicated that the as-deposited material contained P in several oxidation states, consistent with the prior XPS analysis. Relative to the *ex-situ* spectrum, in the *in-situ* and *operando* spectra the spectral features

at 2152.6 eV and 2150.2 eV were attenuated, while the feature at 2144.9 eV, attributed to P in a phosphide form, increased in intensity. These data thus indicate that the oxidized P species were reduced to phosphide during operation, and suggest the active electrocatalyst is predominantly composed of P in a reduced oxidation state. This behavior is consistent with the Raman analysis, wherein signals ascribable to oxidized P species were only observed in the *ex-situ* examination of the as-prepared material. The cumulative data, represented graphically in Figure 4, thus suggest that although *ex-situ* analysis of the electrodeposited film indicated a material composed of multiple phases with Co and P both existing in several oxidation states, the active electrocatalyst is an amorphous material composed of Co in a near-zero valent state and P in a reduced state. A material synthesis that ensures production of solely a metal phosphide phase as the initial film composition therefore does not appear to be necessary for producing an effective CoP-based HER electrocatalyst.

In summary, voltammetric analysis indicated that films electrodeposited from an aqueous solution containing $CoCl_2$ and $NaPO_2H_2$ were active HER electrocatalysts, capable of effecting a -10 mA cm^{-2} current density towards the HER at -$\square$ < 100 mV in 0.500 M H_2SO_4(aq). *Ex-situ* Raman analysis of as-deposited material indicated the presence of several oxidized Co species, including crystalline Co_3O_4, as well as oxygenated P species, but the associated spectroscopic signatures were not observed during *operando* analysis. No phonon scattering was observed during *operando* Raman analysis. *Ex-situ* Co K-edge and P K-edge XANES spectra also indicated the presence of oxidized Co and P species in addition to a near-zero valent Co species and a reduced P species. *Operando* XANES data exhibited a pronounced decrease in the absorption edges of oxidized Co and P species. Additionally, *ex-situ* Co K-edge EXAFS data indicated the presence of a crystalline, oxidized Co-containing phase, but, as in the Raman analysis, this signal was not observed during *operando* analysis. The collective spectroscopic evidence thus indicates that the active electrocatalyst is an amorphous material consisting of Co in a near-zero-valent state and P in a reduced state.

ASSOCIATED CONTENT

Supporting Information

The Supporting Information is available free of charge on the ACS Publications website.

> Details regarding experimental methods, additional standard P K-edge X-ray absorption spectra, and related references (PDF)

AUTHOR INFORMATION

Corresponding Authors

*jyano@lbl.gov
*msoriaga@caltech.edu
*nslewis@caltech.edu

Author Contributions

☼These authors contributed equally (FHS and AIC).

Notes
The authors declare no competing financial interests.

REFERENCES

(1) Ursúa, A.; Gandía, L. M.; Sanchis, P. *Proc. IEEE* **2012**, *100*, 410-426.
(2) Turner, J.; Sverdrup, G.; Mann, M. K.; Maness, P.-C.; Kroposki, B.; Ghirardi, M.; Evans, R. J.; Blake, D. *Int. J. Energy Res.* **2008**, *32*, 379-407.
(3) Cook, T. R.; Dogutan, D. K.; Reece, S. Y.; Surendranath, Y.; Teets, T. S.; Nocera, D. G. *Chem. Rev.* **2010**, *110*, 6474-6502.
(4) Pentland, N.; Bockris, J. O.; Sheldon, E. *J. Electrochem. Soc.* **1957**, *104*, 182-194.
(5) Lee, T. S. *J. Electrochem. Soc.* **1971**, *8*, 1278-1282.
(6) Schuldiner, S. *J. Electrochem. Soc.* **1952**, *99*, 488-494.

(7) McKone, J. R.; Marinescu, S. C.; Brunschwig, B. S.; Winkler, J. R.; Gray, H. B. *Chem. Sci.* **2014**, *5*, 865-878.

(8) Soriaga, M. P.; Baricuatro, J. H.; Cummins, K. D.; Kim, Y.-G.; Saadi, F. H.; Sun, G.; McCrory, C. C. L.; McKone, J. R.; Velazquez, J. M.; Ferrer, I. M.; Carim, A. I.; Javier, A.; Chmielowiec, B.; Lacy, D. C.; Gregoire, J. M.; Sanabria-Chinchilla, J.; Amashukeli, X.; Royea, W. J.; Brunschwig, B. S.; Hemminger, J. C.; Lewis, N. S.; Stickney, J. L. *Surf. Sci.* **2015**, *631*, 285-294.

(9) Zou, X.; Zhang, Y. *Chem. Soc. Rev.* **2015**, *44*, 5148-5180.

(10) Choquette, Y.; Brossard, L.; Lasia, A.; Ménard, H. *Electrochim. Acta* **1990**, *35*, 1251-1256.

(11) Brown, D. E.; Mahmood, M. N.; Man, M. C. M.; Turner, A. K. *Electrochim. Acta* **1984**, *29*, 1551-1556.

(12) McKone, J. R.; Sadtler, B. F.; Werlang, C. A.; Lewis, N. S.; Gray, H. B. *ACS Catal.* **2013**, *3*, 166-169.

(13) Carmo, M.; Fritz, D. L.; Mergel, J.; Stolten, D. *Int. J. Hydrogen Energy* **2013**, *38*, 4901-4934.

(14) Popczun, E. J.; McKone, J. R.; Read, C. G.; Biacchi, A. J.; Wiltrout, A. M.; Lewis, N. S.; Schaak, R. E. *J. Am. Chem. Soc.* **2013**, *135*, 9267-9270.

(15) Shi, Y.; Zhang, B. *Chem. Soc. Rev.* **2016**, *45*, 1529-1541.

(16) Popczun, E. J.; Read, C. G.; Roske, C. W.; Lewis, N. S.; Schaak, R. E. *Agnew. Chem., Int. Ed.* **2014**, *53*, 5427-5430.

(17) Callejas, J. F.; McEnaney, J. M.; Read, C. G.; Crompton, J. C.; Biacchi, A. J.; Popczun, E. J.; Gordon, T. R.; Lewis, N. S.; Schaak, R. E. *ACS Nano* **2014**, *8*, 11101-11107.

(18) Liu, Q.; Tian, J.; Cui, W.; Jiang, P.; Cheng, N.; Asiri, A. M.; Sun, X. *Agnew. Chem., Int. Ed.* **2014**, *53*, 6710-6714.

(19) Jiang, P.; Liu, Q.; Liang, Y.; Tian, J.; Asiri, A. M.; Sun, X. *Agnew. Chem., Int. Ed.* **2014**, *53*, 12855-12859.

(20) Saadi, F. H.; Carim, A. I.; Verlage, E.; Hemminger, J. C.; Lewis, N. S.; Soriaga, M. P. *J. Phys. Chem. C* **2014**, *118*, 29294-29300.

(21) Tyczkowski, J.; Kapica, R.; Łojewska, J. *Thin Solid Films* **2007**, *515*, 6590-6595.

(22) Hadjiev, V. G.; Iliev, M. N.; Vergilov, I. V. *J. Phys. C Solid State Phys.* **1988**, *21*, L199-L201.

(23) Frost, R. L. *Spectrochim. Acta Mol. Biomol. Spectrosc.* **2004**, *60*, 1439-1445.

(24) Mitchell, P. C. H.; Parker, S. F.; Simkiss, K.; Simmons, J.; Taylor, M. G. *J. Inorg. Biochem.* **1996**, *62*, 183-197.

(25) Bell, R. M.; Jeppesen, M. A. *J. Chem. Phys.* **1935**, *3*, 245-247.

(26) Cox, R. A.; Haldna, Ü. L.; Idler, K. L.; Yates, K. *Can. J. Chem.* **1981**, *59*, 2591-2598.

(27) Pourbaix, M. *Atlas of Electrochemical Equilibria In Aqueous Solutions*; Permagon Press: Oxford, 1966.

(28) Bando, K. K.; Wada, T.; Miyamoto, T.; Miyazaki, K.; Takakusagi, S.; Koike, Y.; Inada, Y.; Nomura, M.; Yamaguchi, A.; Gott, T.; Ted Oyama, S.; Asakura, K. *J. Catal.* **2012**, *286*, 165-171.

(29) Kawai, T.; Sato, S.; Chun, W. J.; Asakura, K.; Bando, K. K.; Matsui, T.; Yoshimura, Y.; Kubota, T.; Okamoto, Y.; Lee, Y. K.; Oyama, T. S. *Phys. Scr.* **2005**, *2005*, 822-824.

(30) Koningsberger, D. C.; Mojet, B. L.; van Dorssen, G. E.; Ramaker, D. E. *Top. Catal.* **2000**, *10*, 143-155.

(31) Cargill, G. S.; Cochrane, R. W. *J. Phys. Colloques* **1974**, *35*, C4-269-C264-278.

(32) Chi, G. C.; Cargill Iii, G. S. *J. Appl. Phys.* **1979**, *50*, 2713-2720.

(33) Rundqvist, S. *Acta Chem. Scand.* **1960**, *14*, 1961-1979.

(34) Redman, M. J.; Steward, E. G. *Nature* **1962**, *193*, 867.